

Correlated vortex pinning in Si-nanoparticle doped MgB₂

Ivica Kušević,¹ Emil Babić,¹ Ozren Husnjak,¹ Saeid Soltanian,² Xiaolin Wang,² and Shi Xue Dou²

¹*Department of Physics, Faculty of Science, University of Zagreb, HR-10000 Zagreb, Croatia*

²*Institute for Superconducting and Electronic Materials,
University of Wollongong, NSW 2522, Australia*

(Dated: November 1, 2018)

The magnetoresistivity and critical current density of well characterized Si-nanoparticle doped and undoped Cu-sheathed MgB₂ tapes have been measured at temperatures $T \geq 28$ K in magnetic fields $B \leq 0.9$ T. The irreversibility line $B_{irr}(T)$ for doped tape shows a stepwise variation with a kink around 0.3 T. Such $B_{irr}(T)$ variation is typical for high-temperature superconductors with columnar defects (a kink occurs near the matching field B_ϕ) and is very different from a smooth $B_{irr}(T)$ variation in undoped MgB₂ samples. The microstructure studies of nanoparticle doped MgB₂ samples show uniformly dispersed nanoprecipitates, which probably act as a correlated disorder. The observed difference between the field variations of the critical current density and pinning force density of the doped and undoped tape supports the above findings.

PACS numbers: 74.25.Qt,74.25.Sv,74.62.Dh,74.70.Ad

INTRODUCTION

The discovery of superconductivity in MgB₂ compound [1] has aroused a great deal of interest in the scientific community [2]. Compared to high-temperature superconductors (HTS), MgB₂ has a lower transition temperature $T_c \simeq 39$ K, but its simple composition, abundance of constituents and the absence of weak intergranular links [3, 4, 5] make the MgB₂ a promising material for applications at $T \geq 20$ K, which is above T_c s of conventional superconductors (LTS). Indeed, the simple preparation and rather high critical currents J_c of composite MgB₂ tapes and wires [4, 6, 7, 8, 9] lend strong support to these expectations. Unfortunately, compared to practical LTS (NbTi, Nb₃Sn), MgB₂ exhibits weak flux-pinning [2, 10], which results in strong field dependence of J_c and a low irreversibility field $B_{irr}(4.2 \text{ K}) \approx 8$ T [2].

Several techniques, such as alloying [11, 12, 13], particle irradiation [14, 15, 16, 17] and mechanical processing [9, 18] have been employed in order to improve the flux-pinning in MgB₂, but with limited success. In particular, proton irradiation [14] increased B_{irr} at 20 K, but also suppressed low-field J_c , whereas alloying seems to enhance J_c , but has little effect on B_{irr} [12, 13]. Better results were recently obtained by adding nanoparticles to MgB₂ [19, 20, 21]. It appears that a variety of nanoparticles considerably enhance the flux-pinning in MgB₂ over a wide temperature range $T \leq 30$ K. In particular, the addition of 10 wt% of SiC nanoparticles [20] yielded $B_{irr}(4.2 \text{ K}) \gtrsim 12$ T, which is higher than that of optimized NbTi [22]. The actual mechanism of the flux-pinning enhancement upon nanoparticle doping of MgB₂ is not well understood at present.

Here we present the results for magnetoresistance $R(T, B)$ and critical current $I_c(T, B)$ of MgB₂ tape doped with Si-nanoparticles, which reveal the flux-pinning mechanism associated with nanoparticle doping.

In particular, $B_{irr}(T)$ of doped sample shows a kink at $B_{irr} \approx 0.3$ T, which is the signature of vortex pinning at correlated defects [23], whereas no kink is observed in undoped sample. The variation of critical current and pinning force density $F_p = J_c B$ with the field and temperature also show different pinning mechanisms in doped and undoped MgB₂, respectively.

EXPERIMENTAL PROCEDURES

Cu-sheathed MgB₂ tapes were prepared by in-situ powder-in-tube method [8]. In the doped tape, in addition to Mg and B, 5 wt% of Si-nanoparticles with an average size ~ 50 nm was added. A low sintering temperature (670–690° C) and a short sintering time (several minutes) were employed [21] in order to avoid diffusion of Cu into the MgB₂ core [24]. This resulted in rather porous, low density ($\sim 50\%$) cores. The core cross-sections were elliptical with areas $4.95 \cdot 10^{-3}$ and $4.8 \cdot 10^{-3}$ cm² for the doped and undoped tape, respectively. The sample lengths were approximately 1.5 cm and the voltage and current leads were soldered on Cu-sheathing. The magnetoresistance was measured with low-frequency ac method [5, 15] for $T \geq 28$ K in magnetic field $B \leq 0.9$ T perpendicular to a broad face of the tape and the current direction. $I_{RMS} = 1$ mA was used and the voltage resolution was 0.3 nV. Critical currents were measured on samples used in $R(T, B)$ measurements with the pulse method (sawtooth pulse with duration less than 10 ms and peak current of 200 A [8]).

RESULTS AND DISCUSSION

The variation of the resistance with temperature ($28 \leq T \leq 300$ K) for our undoped and Si-doped tape (Fig. 1)

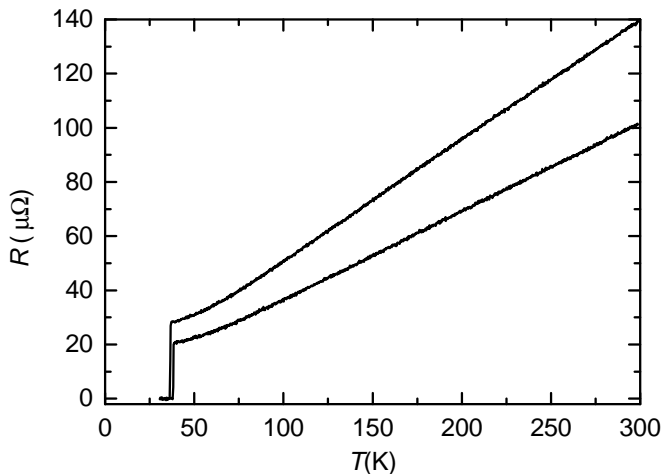


FIG. 1: Temperature variation of the electrical resistance for the undoped (lower) and doped (upper curve) sample.

are typical for Cu-clad MgB_2 wires [24], with a larger resistance of the doped sample due to a larger distance between its voltage contacts.

Fig. 2 compares the superconducting transitions in fields $B \leq 0.9$ T for undoped and doped sample. As in other composite superconductors [25], the shape of these transitions is affected by Cu-sheathing. However, the onset of resistance (hence $T_c(R \rightarrow 0) = T_{c0}$) is not affected by sheathing [25], and the zero-field $T_{c0} = 38.2$ K for the undoped tape (Fig. 2a) is typical for bulk MgB_2 samples [2, 5, 24]. A strong shift of its T_{c0} with magnetic field (i.e. $T_{irr}(B)$) reflects a weak flux-pinning in the undoped MgB_2 . For the doped sample (Fig. 2b), zero-field $T_{c0} = 36.4$ K is lower than that of the undoped one, but the shift of its T_{c0} with field is considerably smaller, which indicates an enhancement of flux-pinning (the expansion of the vortex-solid regime). Furthermore, values of T_{c0} for the doped sample in $B \lesssim 0.3$ T are compressed within a rather narrow temperature interval, whereas those for the undoped one are more evenly spread throughout the explored field range.

Fig. 3 compares the irreversibility fields $B_{irr}(T)$ (defined by using the low-resistivity criterion $\rho_c = 5$ n Ω cm) for our samples. For the undoped tape, both the magnitude and temperature variation of B_{irr} are the same as the literature data for MgB_2 samples [2, 5, 16, 24, 26]. In particular, our values of $B_{irr}(T)$ are equal to those obtained from the onset of the third harmonic in the low-frequency ac susceptibility of a dense MgB_2 sample [26]. Approximately linear, $B_{irr}(T)$ variation for $T \leq 36$ K extrapolates to $B_{irr}(4.2 \text{ K}) \approx 8.4$ T, which is a typical value for bulk MgB_2 [2].

The $B_{irr}(T)$ variation for the doped tape is very different from that of the undoped one (Fig. 3). Here, B_{irr} increases rapidly with decreasing temperature down to 35.5 K, and shows slower, linear variation for $T \leq 35$

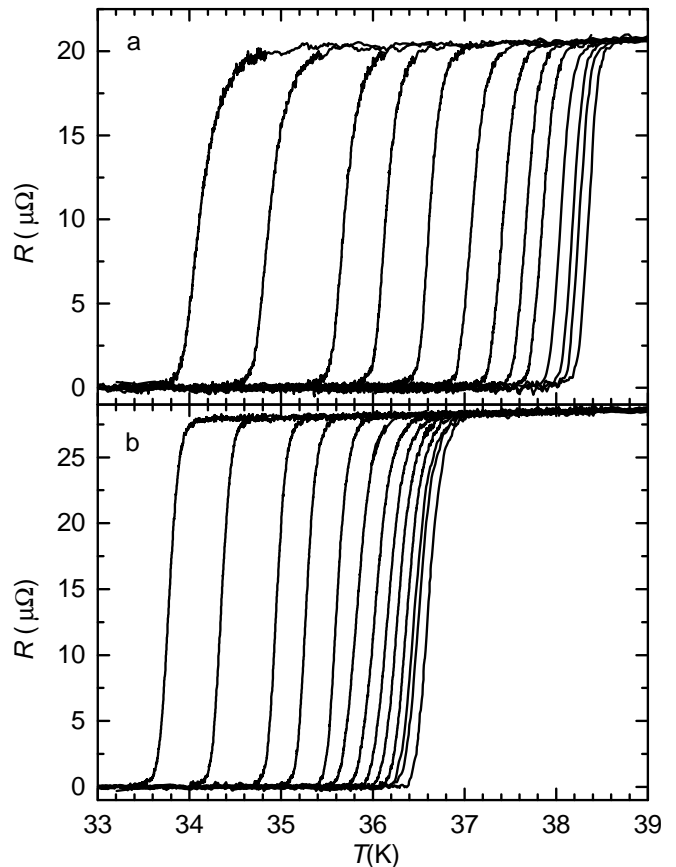


FIG. 2: Temperature variation of the electrical resistance in magnetic fields $B = 0, 0.01, 0.02, 0.04, 0.07, 0.1, 0.14, 0.2, 0.3, 0.4, 0.5, 0.6, 0.7, 0.8$ and 0.9 T for the a) undoped and b) doped sample.

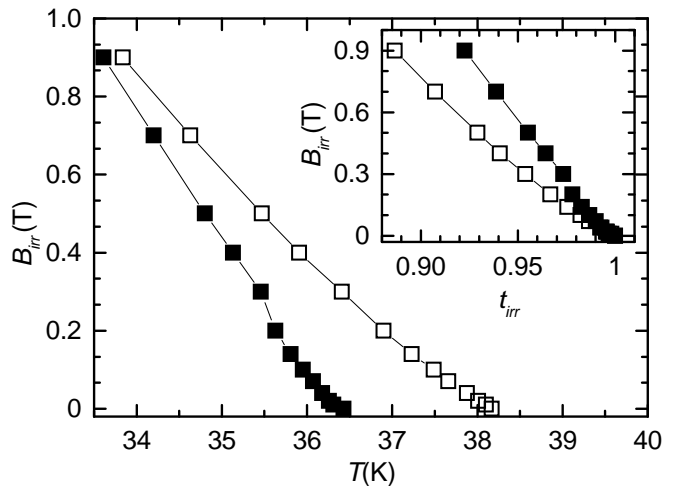


FIG. 3: Temperature dependence of the irreversibility field B_{irr} for the undoped (empty) and doped (full squares) sample. Inset: the same dependence, but vs. the reduced temperature $t_{irr} = T_{irr}(B)/T_{irr}(0)$.

K. Such a stepwise $B_{irr}(T)$ variation is specific for HTS containing columnar defects [23, 27, 28, 29], where the crossover in $B_{irr}(T)$ occurs around the matching field B_ϕ , which is the field at which the vortex and columnar defect density n_ϕ are equal ($B_\phi = n_\phi \Phi_0$, Φ_0 being the flux quantum [28, 29]). This crossover occurs because the pinning of interstitial vortices for $B_{irr} > B_\phi$ is less weaker than for vortices residing onto the columns for $B_{irr} < B_\phi$.

From our crossover field $B_c \approx B_{irr}(35.5 \text{ K}) \simeq 0.3 \text{ T}$ we estimate $n_\phi \approx 1.4 \cdot 10^{14} \text{ m}^{-2}$, and the average distance between defects $\sim 80 \text{ nm}$. The microstructural studies of the nanoparticle doped MgB_2 [19, 20, 21] show finely dispersed precipitates within the MgB_2 matrix with sizes $\sim 10 \text{ nm}$. For Si and SiC doped MgB_2 [20, 21] these precipitates are mainly Mg_2Si phase, and their average spacing is comparable to that estimated above. Therefore in our tape Mg_2Si nanoprecipitates, resulting from the reaction of Si-nanoparticles and Mg during the sintering, act analogously to columnar defects in HTS. This outcome appears rather surprising considering different nature and geometries of precipitates and columns, as well as the different nature of vortices [23, 30] in these materials. However, the matching effects are common in type-II superconductors [31] and are not specific only to HTS.

A linear variation of $B_{irr}(T)$ for $T \leq 35 \text{ K}$ in the doped sample extrapolates to $B_{irr}(4.2 \text{ K}) \simeq 11.5 \text{ T}$, which is consistent with the other results for nanoparticle-doped MgB_2 [19, 20, 21], and is higher than $B_{irr}(4.2 \text{ K})$ for NbTi. However, for $T > 33 \text{ K}$, B_{irr} of the doped sample is lower than that for the undoped sample, which is entirely due to its lower zero-field T_{c0} . Indeed, a plot of B_{irr} vs. reduced temperature $t_{irr} = T_{irr}(B)/T_{irr}(0)$ for both samples (inset to Fig. 3) shows that for all values of t_{irr} , B_{irr} of the doped sample is higher than that of the undoped one. Therefore, vortex pinning in nanoparticle doped MgB_2 is enhanced with respect to that in undoped MgB_2 at all reduced temperatures.

Different vortex pinning mechanisms in our tapes imply also different field variations of their J_c and $F_p = J_c B$. Fig. 4 compares the $J_c(B)$ variations of our samples for $T \geq 33 \text{ K}$. The undoped tape (Fig. 4a) shows approximately exponential $J_c(B)$ variation, which is typical for MgB_2 samples [2, 10, 14, 20]. At low temperatures (high I_c), large self-field $\mu_0 H_s$ ($H_s \simeq I_c/c$, where c is the circumference of the core) makes $J_c(B < \mu_0 H_s)$ nearly constant, whereas at elevated fields ($B \rightarrow B_{irr}$) J_c rapidly decreases to zero. From the experimental $J_c(B, T)$ curves (Fig. 4a) we obtained $F_p(B, T)$ ones, from which we determined the fields $B_{max}(T)$ at which the volume pinning force density reaches its maximum value $F_{pmax} = J_c B_{max}$. The field B_{max} is an important parameter of the vortex pinning within the vortex-solid phase. In particular, in the case of dominant vortex pinning mechanism, the ratio B_{max}/B_{irr} may re-

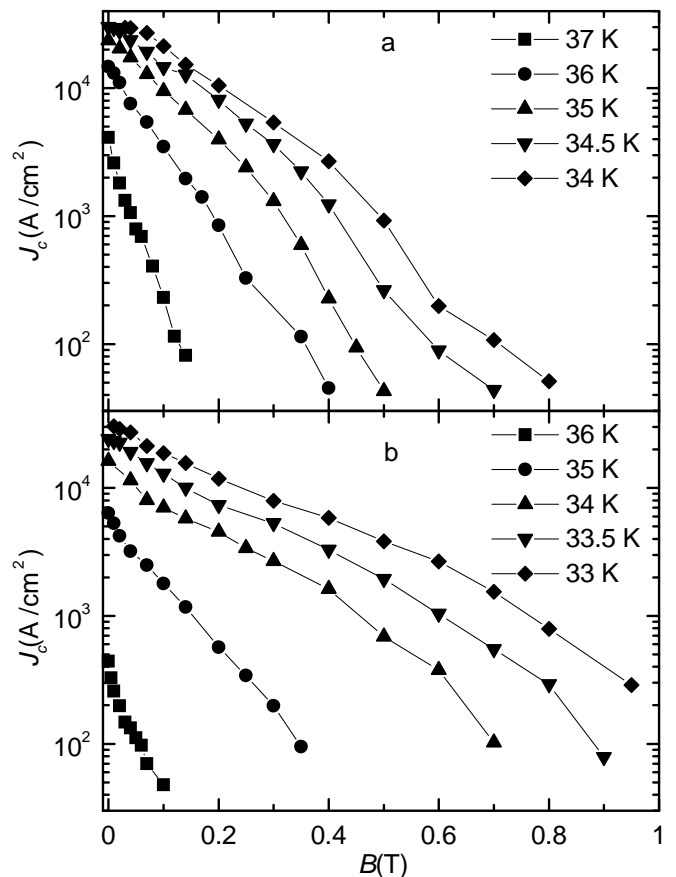


FIG. 4: Dependence of the critical current density J_c on magnetic field B at denoted temperatures for the a) undoped and b) doped sample.

veal this mechanism. For the undoped tape we found $B_{max}/B_{irr} \approx 0.21$, which is similar to that observed in Nb_3Sn [32] and is consistent with a commonly accepted grain boundary pinning mechanism for a bulk MgB_2 [3]. In spite of a probably common vortex pinning mechanism in both bulk MgB_2 and Nb_3Sn , vortex pinning in MgB_2 is apparently weaker (lower B_{max} and B_{irr}) than that in Nb_3Sn . The probable reason for that are larger grains, clean and narrow grain boundaries, and quite a large coherence length [30] in MgB_2 .

The $J_c(B)$ variation of nanoparticle doped MgB_2 sample (Fig. 4b) is very different from that for the undoped tape (Fig. 4a). The S-shaped $J_c(B)$ curves of the doped tape are reminiscent of those observed in HTS films, tapes and crystals containing columnar defects [23]. Further, for the same reduced temperature $t = T/T_c$, the decrease of J_c with B in the doped tape is considerably smaller than that for the undoped one. Accordingly, the fields $B_{max}(t)$ are enhanced with respect to those of the undoped tape, which shows that nanoparticle doping enhances vortex pinning throughout the vortex-solid regime [23]. Furthermore, the enhancement of $B_{max}(t)$ in the doped tape is larger than that of

$B_{irr}(t)$, which results in $B_{max}(t)/B_{irr}(t) \approx 0.29$ for the doped tape. Such B_{max}/B_{irr} ratio is unlikely to arise only from the grain boundary pinning [32] and was earlier observed for HTS tapes [33] with a modest density of columnar defects ($B_\phi \lesssim 0.2$ T). Therefore, we propose that $B_{max}/B_{irr} \approx 0.29$ arises from the competition of two pinning mechanisms (for example, a grain boundary pinning and a core pinning at nanoprecipitates) as was the case in HTS tapes. A detailed investigation of $J_c(B)$ curves for a number of temperatures extending over a broad temperature range (which requires $I > 200$ A) is necessary in order to solve this problem.

In spite of 50% porosity, our tapes have large self-field J_{cs} (Fig. 4), which increase rapidly with decreasing temperature ($J_c(t) \simeq J_c(0)(1-t)^n$, with $n \approx 1.5$). In particular, the observed $J_c(0.9T_c) \approx 40$ kA/cm² for both tapes extrapolate to $J_c(20$ K) ≈ 350 kA/cm², the value which was confirmed by the magnetic measurements of $J_c(20$ K) [21]. Therefore, fully dense MgB₂ tapes are expected [5, 19] to reach $J_c(20$ K) $\sim 10^6$ A/cm², which is above $J_c(4.2$ K) for the best Bi2223/Ag tapes.

In summary, we have shown that a uniform dispersion of Mg₂Si nanoprecipitates (resulting from the addition of Si-nanoparticles to Mg and B powders [20, 21]) not only enhances the flux-pinning in MgB₂ samples, but also introduces an additional pinning mechanism. In particular, we observed a step-wise variation of $B_{irr}(T)$ in nano-Si doped MgB₂ tape with a kink around $B_\phi \simeq 0.3$ T, which is reminiscent of the vortex pinning at correlated disorder in HTS [23, 27, 28, 29]. We also observed a corresponding difference in the shapes of $J_c(B)$ and $F_p(B)$ curves for the doped and undoped tape respectively. Although our results were obtained for MgB₂ tape doped with Si nanoparticles only, we believe that the above conclusions hold also for other MgB₂ samples doped with different types of nanoparticles [19, 20, 21], providing that these nanoparticles form uniformly dispersed non-superconducting nanoprecipitates.

We thank Ms Mino Delfany for the preparation of samples.

[1] J. Nagamatsu, N. Nagakawa, T. Muranaka, Y. Zenitani, and J. Akimitsu, *Nature* **410**, 63 (2001).
 [2] C. Buzea and T. Yamashita, *Supercond. Sci. Tech.* **14**, R115 (2001).
 [3] D. Larbalestier et al., *Nature* **410**, 186 (2001).
 [4] B. Glowacki, M. Majoros, M. Vickers, J. Evetts, Y. Shi, and I. McDougall, *Supercond. Sci. Tech.* **14**, 193 (2001).
 [5] I. Kušević, Ž. Marohnić, E. Babić, Đ. Drobac, X. L. Wang, and S. X. Dou, *Solid State Commun.* **122**, 347 (2002).
 [6] G. Grasso, A. Malagoli, C. Ferdeghini, S. Roncallo, V. Braccini, A. S. Siri, and M. R. Cimberle, *Appl. Phys. Lett.* **79**, 230 (2001).
 [7] S. Jin, H. Mavoori, C. Bower, and R. B. van Dover, *Nature* **411**, 563 (2001).

[8] S. Soltanian, X. L. Wang, I. Kušević, E. Babić, A. H. Li, H. K. Liu, E. W. Collings, and S. X. Dou, *Physica C* **361**, 84 (2001).
 [9] H. L. Suo, C. Beneduce, M. Dhallè, N. Musolino, J. Y. Genoud, and R. Flükiger, *Appl. Phys. Lett.* **79**, 3116 (2001).
 [10] D. K. Finnemore, J. E. Ostenson, S. L. Bud'ko, G. Laperot, and P. C. Canfield, *Phys. Rev. Lett.* **86**, 2420 (2001).
 [11] C. B. Eom et al., *Nature* **411**, 558 (2001).
 [12] Y. Feng, Y. Zhao, Y. P. Sun, F. C. Liu, B. Q. Fu, L. Zhou, C. H. Cheng, N. Koshizuka, and M. Murakami, *Appl. Phys. Lett.* **79**, 3983 (2001).
 [13] M. R. Cimberle, M. Novak, P. Manfrinetti, and A. Palenzona, *Supercond. Sci. Technol.* **15**, 43 (2002).
 [14] Y. Bugoslavsky, L. F. Cohen, G. K. Perkins, M. Polichetti, T. J. Tate, R. G. William, and A. D. Caplin, *Nature* **411**, 561 (2001).
 [15] E. Babić, Đ. Miljanić, K. Zadro, I. Kušević, Ž. Marohnić, Đ. Drobac, X. L. Wang, and S. X. Dou, *FIZIKA A* **10**, 87 (2001).
 [16] M. Eisterer, B. A. Glowacki, H. W. Weber, L. R. Greenwood, and M. Majoros, *Supercond. Sci. Technol.* **15**, 1088 (2002).
 [17] S. Okayasu et al., *Physica C* **382**, 104 (2002).
 [18] A. Gumbel, J. Eckert, G. Fuchs, K. Nenkov, K. H. Müller, and L. Schultz, *Appl. Phys. Lett.* **80**, 2725 (2002).
 [19] J. Wang, Y. Bugoslavsky, A. Berenov, L. Cowey, A. D. Caplin, L. F. Cohen, J. L. M. Driscoll, L. D. Cooley, X. Song, and D. C. Larbalestier, *Appl. Phys. Lett.* **81**, 2026 (2002).
 [20] S. X. Dou, S. Soltanian, J. Horvat, X. L. Wang, S. H. Zhou, M. Ionescu, H. K. Liu, P. Munroe, and M. Tomsic, *Appl. Phys. Lett.* **81**, 3419 (2002).
 [21] X. L. Wang, S. Soltanian, M. James, W. W. Jao, M. J. Qin, J. Horvat, H. K. Liu, and S. X. Dou, *Physica C* (2003), to be published.
 [22] C. Meingast and D. C. Larbalestier, *J. Appl. Phys.* **66**, 5971 (1989).
 [23] G. Blatter, M. V. Feigel'man, V. B. Geshkenbein, A. I. Larkin, and V. M. Vinokur, *Rev. Mod. Phys.* **66**, 1125 (1994).
 [24] M. Majoros, B. A. Glowacki, and M. E. Vickers, *Supercond. Sci. Technol.* **15**, 269 (2002).
 [25] E. Babić, I. Kušević, S. X. Dou, H. K. Liu, and Q. Y. Hu, *Phys. Rev. B* **49**, 15312 (1994).
 [26] D. di Gioacchino, U. Gambardella, P. Tripodi, and G. Grimaldi, *Supercond. Sci. Technol.* **16**, 534 (2003).
 [27] L. Krusin-Elbaum, L. Civale, G. Blatter, A. D. Marwick, F. Holtzberg, and C. Feild, *Phys. Rev. Lett.* **72**, 1914 (1994).
 [28] C. J. van der Beek, M. Konczykowski, V. M. Vinokur, T. W. Li, P. H. Kes, and G. W. Crabtree, *Phys. Rev. Lett.* **74**, 1214 (1995).
 [29] A. Daignère, A. Maignan, V. Hardy, and C. Simon, *Supercond. Sci. Technol.* **14**, 659 (2001).
 [30] M. R. Eskildsen, M. Kugler, S. Tanaka, J. Jun, S. M. Kazakov, J. Karpinski, and Ø. Fischer, *Phys. Rev. Lett.* **89**, 187003 (2002).
 [31] J. Petermann, *Z. Metall.* **61**, 724 (1970).
 [32] D. Dew-Hughes, *Philos. Mag. B* **55**, 459 (1987).
 [33] E. Babić et al., *Solid State Commun.* **118**, 607 (2001).